AGU PUBLICATIONS

Geophysical Research Letters

RESEARCH LETTER
10.1002/2014GL059976

Key Points:
- Driving and basal stress of both ice sheets have organized spatial patterns
- Basal sliding occurs over substantially larger areas than previously recognized
- Organized patterns are caused by processes variable on short time scales

Supporting Information:
- Readme
- Text S1
- Figure S1
- Figure S2
- Figure S3
- Figure S4
- Figure S5
- Figure S6
- Figure S7
- Figure S8
- Figure S9

Correspondence to:
O. V. Sergienko,
osergien@princeton.edu

Citation:
Sergienko, O. V., T. T. Creyts, and R. C. A. Hindmarsh (2014), Similarity of organized patterns in driving and basal stresses of Antarctic and Greenland ice sheets beneath extensive areas of basal sliding, *Geophys. Res. Lett.*, *41*, 3925–3932, doi:10.1002/2014GL059976.

Received 21 MAR 2014
Accepted 29 APR 2014
Accepted article online 3 MAY 2014
Published online 10 JUN 2014

Similarity of organized patterns in driving and basal stresses of Antarctic and Greenland ice sheets beneath extensive areas of basal sliding

O. V. Sergienko[1], T. T. Creyts[2], and R. C. A. Hindmarsh[3]

[1]GFDL/AOS Princeton University, Princeton, New Jersey, USA, [2]Lamont-Doherty Earth Observatory Columbia University, Palisades, New York, USA, [3]Science Programmes, British Antarctic Survey, Cambridge, UK

Abstract The rate of ice transport from the interior of ice sheets to their margins, and hence the rate with which it contributes to sea level, is determined by the balance of driving stress, basal resistance, and ice internal deformation. Using recent high-resolution observations of the Antarctic and Greenland ice sheets, we compute driving stress and ice deformation velocities, inferring basal traction by inverse techniques. The results reveal broad-scale organization in 5–20 km band-like patterns in both the driving and basal shear stresses located in zones with substantial basal sliding. Both ice sheets experience basal sliding over areas substantially larger than previously recognized. The likely cause of the spatial patterns is the development of a band-like structure in the basal shear stress distribution that is the results of pattern-forming instabilities related to subglacial water. The similarity of patterns on the Greenland and Antarctic ice sheets suggests that the flow of ice sheets is controlled by the same fundamental processes operating at their base, which control ice sheet sliding and are highly variable on relatively short spatial and temporal scales, with poor predictability. This has far-reaching implications for understanding of the current and projection of the future ice sheets' evolution.

1. Introduction

Ice sheet flow, which is gravity-driven, changes with changes in conditions at the ice/bed interface (e.g., slipperiness as result of melting/refreezing of water and topography as a result of bed deformation), which in turn cause changes in ice thickness and surface elevation slope, and consequently in the driving stress [*Van der Veen*, 1999]. Equally, changes in the driving stress due to external forcings (e.g., changes in surface ablation/accumulation) change the rates of flow and conditions at the bed. Understanding the physical processes governing spatial and temporal variability of the driving and basal shear stresses is imperative in understanding the behavior of ice sheets (past and present) and for projections of their evolution under changing climate.

Recent advances in cryospheric remote-sensing systems (satellite and air-borne based) have yielded a wealth of high spatial resolution observations of the Greenland and Antarctic ice sheets. The recently released data sets of Greenland [*Bamber et al.*, 2013] and Antarctica surface and bed topography [*Bamber et al.*, 2009; *Fretwell et al.*, 2013] and surface ice flow [*Joughin et al.*, 2010; *Rignot et al.*, 2011] have unprecedentedly high resolutions of 1 km, 500 m, and 900 m, respectively. Taking advantage of such high spatial resolution data products, we investigate spatial variability of the three components of the ice momentum balance—the driving and basal stress and ice internal deformation—that determine the rate of ice sheets' flow, and the consequent ice discharge into surrounding oceans.

2. Driving Stress

The driving stress, τ_d, can be directly computed using observed values of ice thickness and surface slopes:

$$\tau_d = \rho g H \left|\vec{\nabla} S\right| \tag{1}$$

where ρ is ice density, g is the acceleration due to gravity, H is ice thickness, $\vec{\nabla}$ is the gradient operator, and S is ice surface elevation. The driving stress, τ_d, computed with these data (Figure 1) appears to have strong similarities on the two ice sheets, on both large and small spatial scales. On the ice sheet scale, driving stress

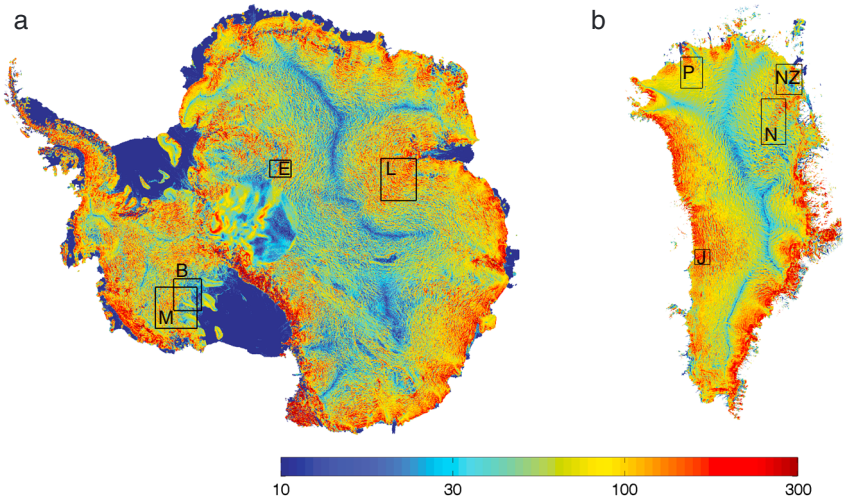

Figure 1. Driving stress (kPa) of (a) Antarctic ice sheet and (b) Greenland ice sheet. Rectangles outline areas where inversion for basal traction were preformed. Antarctica: B, Bindschadler Ice Stream; M, MacAyeal Ice Stream; E, unnamed location at ~40°E, 84°S; L, Lambert Ice Steam. Greenland: P, Petermann Glacier; J, Jakobshavn Isbræ; NZ, 79 North and Zachariae glaciers; N, North-East Greenland Ice Stream (NEGIS). Close-ups of the driving stress in these areas are shown in Figures 2 (left column) and 3 (left column).

progressively increases from zero at ice divides toward the ice sheet margins, and falls to almost zero over floating ice shelves (Figure 1a).

On spatial scales of ~5–20 km, the new data sets show that there is high variability in the driving stress distributions in grounded ice (Figures 2–3, left columns). In both ice sheets, the driving stress organizes into distinct bands of high values that are up to an order of magnitude greater than the stress between the bands. Figure S1 in the supporting information summarizes the spatial characteristic of the high driving-stress bands for selected regions in Antarctica and Greenland (Figures 2–3, left columns). The predominant orientation of these bands is transverse to the ice flow direction. These band-like patterns are associated with and are primarily due to similar patterns in the surface slopes, $\vec{\nabla}S$ (Figures S2–S3). The surface slopes show large variations across the bands, about an order of magnitude change . The corresponding surface undulations have ~30–80 m amplitudes, depending on locations, with the largest ones observed on the Lambert Ice Stream and the smallest on an unnamed location at ~40°E and ~84°S in Antarctica and Petermann Glacier in Greenland.

The similarity of the driving-stress (and surface slope) patterning in both ice sheets suggests that it is unlikely to arise from external causes, as wind and precipitation patterns that could produce such surface undulations are variable across the individual ice sheets and drastically different between them. More likely, these spatial patterns stem from the ice sheets' internal dynamics.

3. Basal Shear Stress

In order to understand the generating processes of such spatially organized variability in the driving stress, we analyze the basal resistance component of ice momentum balance. While surface measurements are sufficient to compute driving stress, basal drag cannot be estimated from surface observations and measurements on ice sheet-wide scales are logistically impossible. Inverse methods [e.g., *MacAyeal*, 1992; *Goldberg and Sergienko*, 2011] provide the necessary means to infer basal conditions under various ice streams [e.g., *Joughin et al.*, 2004; *Sergienko et al.*, 2008]. As the driving stress is highly spatially variable (Figures 2–3, left columns), the inverse model requires even higher horizontal resolution (a fraction of the local ice thickness), and the ability to account for all modes of ice deformation in three dimensions in order to satisfy the governing Stokes equations. It is not computationally feasible to perform such high-resolution three-dimensional inversions for continental ice sheets. Consequently, regional inversions are performed for parts of the Antarctic and Greenland ice sheets (black rectangles in Figure 1), in areas where banding in the driving stress was observed.

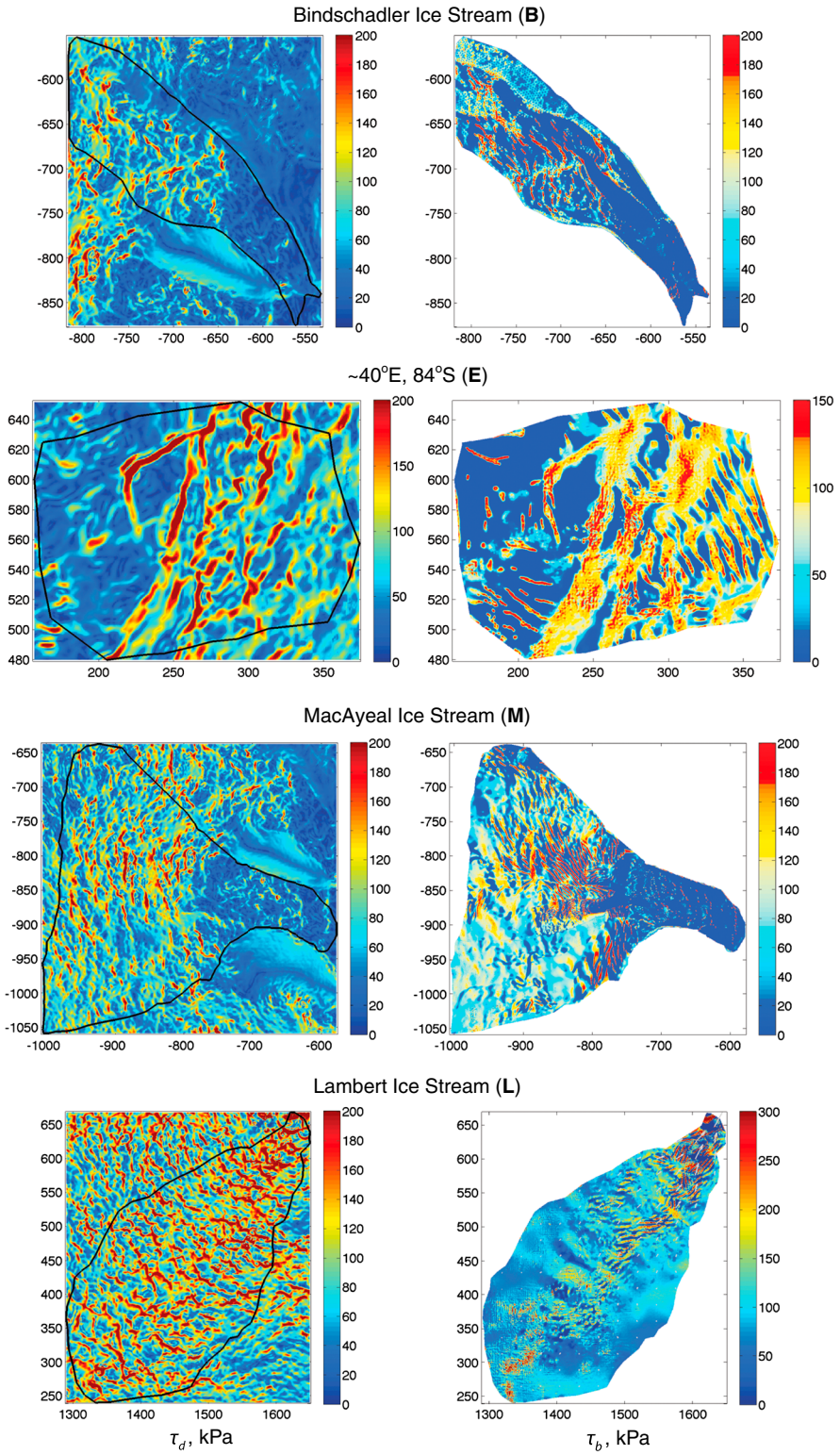

Figure 2. (left column) Driving stress, τ_d (kPa), and (right column) basal shear stress, τ_b (kPa), for selected areas of Antarctic ice sheet.

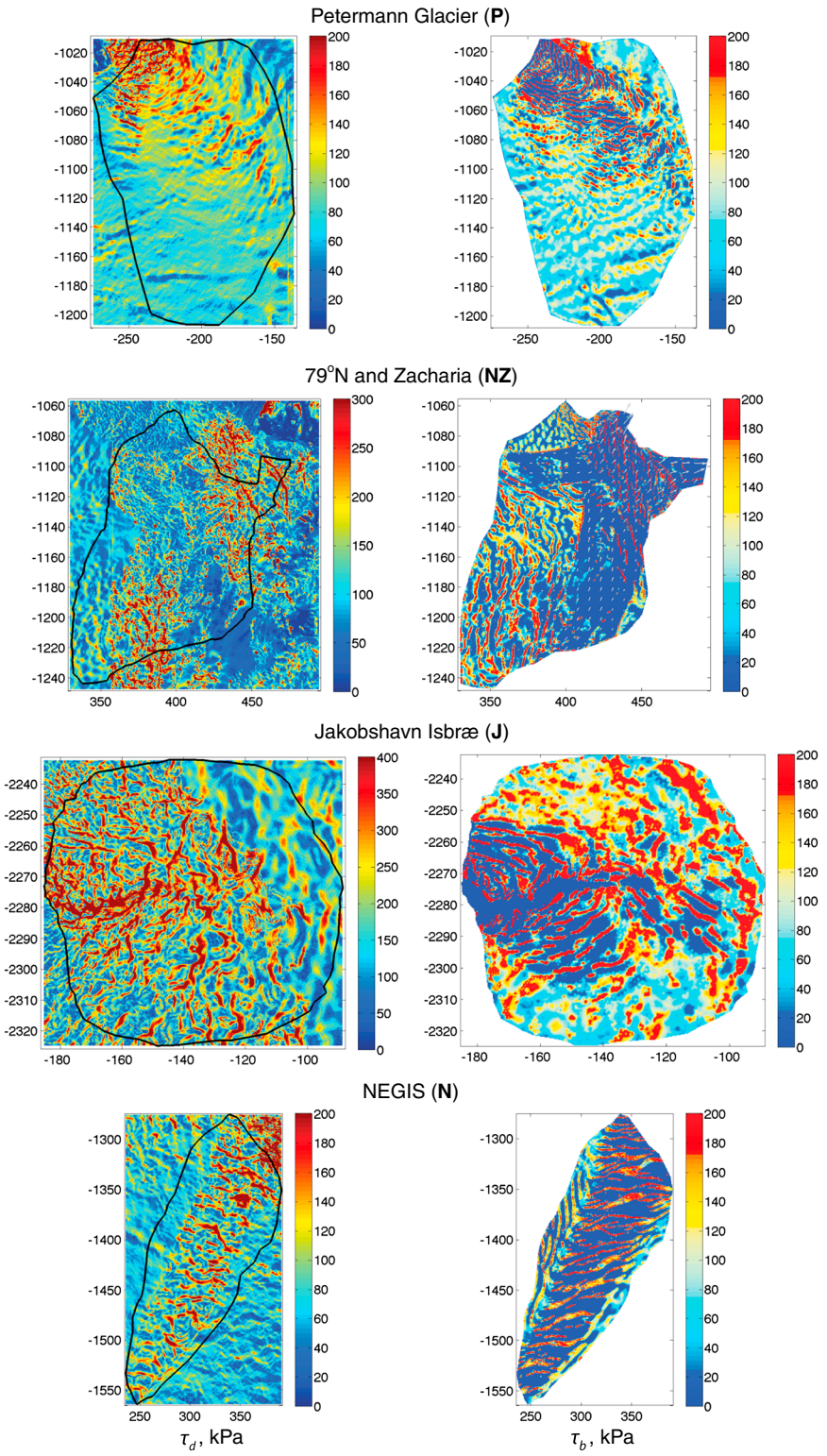

Figure 3. (left column) Driving stress, τ_d (kPa), and (right column) basal shear stress, τ_b (kPa), for selected areas of Greenland ice sheet.

The chosen regions encompass a wide range of characteristics. Bedrock elevation is both above and below sea level, surface ice flow varies by several order of magnitudes between locations and also within selected locations (Figures S4–S7), while the driving stress has a variety of spatial patterns (Figures 2–3, left columns). The locations in Antarctica are the Bindschadler and MacAyeal ice streams in the West Antarctica (denoted by B and M in Figure 1a), an unnamed location at ~40°E and ~84°S and Lambert Ice Stream in the East Antarctica (denoted by E and L in Figure 1a). In Greenland, the locations are Jakobshavn Isbræ and area surrounding it, Petermann Glacier, 79 North and Zachariae glaciers, and the North-East Greenland Ice Stream (NEGIS), denoted by J, P, NZ, and N in Figure 1b, respectively. Inversions for basal shear at these locations used the data sets described above, observed ice surface velocities [*Rignot et al.*, 2011; *Joughin et al.*, 2010] and a recently developed inverse model [*Sergienko and Hindmarsh*, 2013] (detailed description of the inversion procedure is in Text S1, section 1). The spatial patterns obtained are robust with respect to errors in the input data and the specifics of the inversion procedure (supporting information and *Sergienko and Hindmarsh* [2013]).

The inverted basal shear distributions (Figures 2–3, right columns) also exhibit a band-like spatial structure similar to those observed in the driving stress. Areas of high basal traction alternate with areas of low basal traction at all locations where inversions were performed. Areas where the bands with high driving stress are absent or occur less frequently include the trunks of Bindschadler and MacAyeal ice streams in Antarctica (Figure 2) and 79 North and Zachariae glaciers in Greenland (Figure 3). In these locations, there are distinct, elongated structures with very high basal shear (~300 kPa) that lie within large areas with basal shear close to zero. These spatial patterns are similar to ones inferred in inversions of basal shear distribution on Pine Island and Thwaites glaciers (Antarctica) [*Sergienko and Hindmarsh*, 2013]. Figure S8 summarizes the spatial characteristics of the basal shear spatial distributions.

It is remarkable that all locations where inversions have been performed exhibit similar basal shear patterns on small (~5–20 km) spatial scales. Bed topography is not a strong control on all locations and distributions of the basal shear patterns (Figures S4–S5). In some locations, the ribs are concentrated within topographic lows (MacAyeal Ice Stream in Antarctica and NEGIS in Greenland), while in other locations, they are concentrated in local topographic highs (Bindschadler Ice Stream in Antarctica and the flanks of Jakobshavn Isbræ in Greenland). At all locations, the basal friction bands and distinct ribs locate in areas characterized by the high driving-stress bands (Figures 2–3). However, the spatial patterns of the driving and basal stresses do not mimic each other at all locations: the basal friction spatial structures are oriented at ~10–40° angle with respect to the driving-stress structures and, in some locations, span several of them (Figures S5–S8). While the colocation of highs in the driving stress with highs in the basal shear stress is expected, the details of their spatial distributions are not. Although the individual basal shear ribs are nonaligned with the driving-stress bands, in many areas, the basal shear ribs are parallel to each other and organized in echelons that span individual driving-stress bands (e.g., Figures S6–S7).

Where ice flows over beds with heterogeneous basal conditions (topography and basal resistance), it produces undulations on the ice surface that affect spatial variability of the surface slopes and, as a result, the local driving stress [e.g., *Schoof*, 2002; *Gudmundsson*, 2003; *Sergienko*, 2013]. Spatial patterns of heterogeneous basal conditions and resulting surface undulations are not identical, with the surface undulations having a larger spatial extent [*Sergienko*, 2012]. Moreover, multiple distinct topographic undulations or areas with strong basal resistance have cumulative effects on ice flow, and the produced surface undulations have more complicated patterns than the basal patterns. We demonstrate this using idealized simulations of ice flow over several ribs with high basal traction organized in distinct echelons and aligned at 45° to the main direction of ice flow (Text S1, section 2). The simulations show that such spatial distributions of basal traction produce surface undulations, and, as a result, spatially variable driving stress with distinct bands oriented across ice flow (Text S1, section 2).

In view of this, we suggest that the most likely origin of band-like spatial structure in the ice sheets' driving stress is the band-like spatial distribution of the basal shear stress. As the spatial patterns of the driven stress of the areas where inversions were performed are similar to other areas of the two ice sheets, we hypothesize that the band-like patterns in the basal shear stress are widespread under both ice sheets. This implies that many parts of ice sheets where the driving-stress bands occur are experiencing basal sliding.

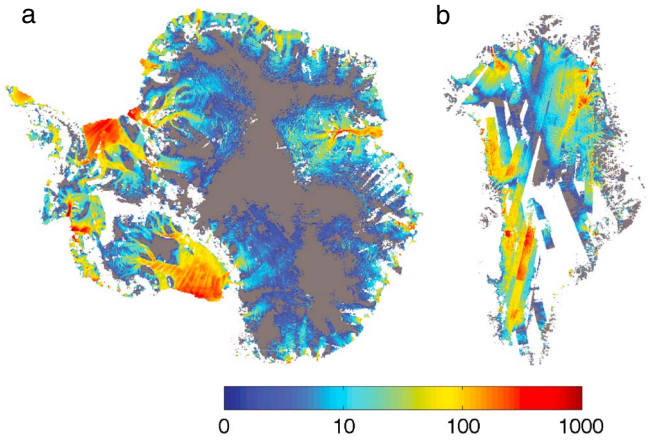

Figure 4. Basal sliding (a) Antarctic ice sheet and (b) Greenland ice sheet. Colors show the ratio of inferred basal speed, $|\mathbf{u}_b|$ to errors in the observed surface speed [*Rignot et al.*, 2011; *Joughin et al.*, 2010]. This ratio indicates the level of confidence in inferred basal sliding—the higher the value, the greater the likelihood of sliding at a particular location. Grey patches indicate areas where no basal sliding can be demonstrated. Here the ratio is less than 1 indicating that the likelihood of sliding is small. The basal velocity $|\mathbf{u}_b| = |\mathbf{u}_{\text{obs}} - \mathbf{u}_{\text{def}}|$, where $|\mathbf{u}_{\text{obs}}|$ are magnitudes of observed surface velocities [*Rignot et al.*, 2011; *Joughin et al.*, 2010] and $|\mathbf{u}_{\text{def}}|$ are computed deformational velocities at ice surface. Detailed description of the computational procedure is in Text S1, section 3.

4. Ice Internal Deformation and Basal Sliding

Ice flow is thought of as a combination of internal deformation and sliding occurring at the ice bed. We can verify the hypothesis of the widespread basal sliding by computing the deformational velocities (difference between surface and basal velocities), accounting for the effect of temperature on deformation, within the ice sheets and comparing them with observed surface velocities (Text S1, section 3). As Figures 4 and S9 show, the driving-stress bands are located in areas where basal sliding is substantial. These results have two important consequences. First, the presence of the driving-stress bands can be indicative of the band-like patterns in the basal shear and basal sliding. Second, the areas of the ice sheets that experience significant basal sliding are substantially larger than previously recognized, e.g., Northern Greenland and large areas of East Antarctica.

Basal sliding is traditionally attributed to the presence of subglacial water. Widespread indications of its presence has been observed underneath most of Antarctica [*Wingham et al.*, 2006; *Wolovick et al.*, 2013; *Engelhardt et al.*, 1990] and Greenland [*Oswald and Gogineni*, 2012], where in addition to subglacial water, surface meltwater can reach the bed in ablation zones [*Catania and Neumann*, 2010]. Subglacial water flow is controlled by the gradient of hydraulic potential [*Shreve*, 1972]

$$\vec{\nabla}\Phi = \rho g \vec{\nabla} S + \left(\rho_w - \rho\right) g \vec{\nabla} B, \tag{2}$$

where ρ_w is water density and $\vec{\nabla} B$ is bed slope. Since the hydraulic potential gradient is dominated by the surface slope, $\vec{\nabla} S$, its spatial variability closely mimics spatial variability of the driving stress, whose spatial variability is dominated by the surface slope as well (Figures S2–S3).

5. Discussion

Rib-like basal resistance patterns could be a result of several distinct mechanisms occurring near or at the ice-bed interface. The offset between the driving stress and basal resistance bands observed in most cases suggests the operation of dynamical processes at the bed, mediated by mechanical coupling within the ice sheet. However, in some instances, the colocation of resistance with driving stress suggests a controlling relationship to basal topography and so the ice surface structure is likely to be static. For example, in the area at ~40°E and ~84°S (Figure 2), colocation of resistance and driving stress appears to correspond well to topography there (Figures S4b). Owing to the correlation between driving stress and gradient in hydraulic potential, changes in the driving stress could affect sliding by changing water availability or water distribution along the bed. Similarly, subglacial water can result in till weakening [*Iverson*, 2010], or erosion and deposition of sediments near the bed either through till movement [*Hindmarsh*, 1998; *Tulaczyk et al.*, 2001;

Smith et al., 2007] or glaciofluvial processes [*Creyts et al.*, 2013]. Since many of these mechanisms occur over length scales substantially less than ice thickness, our inversions are unable to distinguish between such processes, and contrasts in ice rheology [*Dahl-Jensen et al.*, 2013] or patterns of freezing and thawed beds might be equally responsible. With the exception of topography, all of these mechanisms could allow the basal resistance to change on decadal time scales.

The occurrence of regular patterning at the bed is a fingerprint of a dynamical instability [*Sergienko and Hindmarsh*, 2013]. The characteristic scales of the ribs are substantially smaller (~5–20 km or ~ 4–6 local ice thicknesses) than previously observed structures in basal resistance. If formation time is related to transit time of the ice over them, their typical timescales will be decadal to centurial. Regardless of the mechanism, these patterns are likely a manifestation of processes that are highly variable on relatively short spatial and temporal scales. The implications of this are far-reaching, as pattern-forming instabilities are often one manifestation of complex dynamical systems with poor predictability. Understanding the pattern-forming mechanism is therefore critical to understanding future behavior of the ice sheets.

A substantial challenge in understanding such instabilities lies in constructing the long-term variability and how these relate to the expected mean flow conditions of the ice sheet. Borehole measurements of subglacial conditions [*Meierbachtol et al.*, 2013; *Engelhardt and Kamb*, 1997] can capture the temporal variability, but lack the spatial extent to understand development of basal resistance. Broader scale radar [*Schroeder et al.*, 2013; *Wolovick et al.*, 2013] and seismic investigations [*Peters et al.*, 2006; *King et al.*, 2007] give insight into spatial structure but lack the temporal resolution to understand how the ice-bed geometry and properties evolve. Because the patterns are found across the ice sheets, the development of the instabilities affects the broad-scale ice flow with the ribs being the best evidence so far of these instabilities.

Alternative sources of evidence with high spatial detail come from the deglaciated beds of the ice sheets that covered northern America and Eurasia, which exhibit similar features to the inversions for basal resistance ribs beneath the Greenland and Antarctica [*Sergienko and Hindmarsh*, 2013]. These are possibly related to geomorphological structures ("mega-ribs") found at locations of the former Laurentide Ice Sheet formed during Last Glacial Maximum [*Greenwood and Kleman*, 2010]. Pattern forming mechanisms have been proposed for the development of the somewhat smaller ribbed moraines [*Dunlop et al.*, 2008] as well as the very different drumlins [*Smalley and Unwin*, 1968; *Clark*, 2010]. In addition, geomorphological features in Marguerite Bay [*Cofaigh et al.*, 2005] and Pine Island Bay [*Nitsche et al.*, 2013] suggest a complex relationship between ice flow and basal properties.

6. Conclusions

The widespread occurrence of rib-like patterns in driving stress and in basal resistance suggests that despite the drastic differences between the Antarctic and Greenland ice sheets (e.g., latitude, geology, geometry, atmospheric conditions, and climate history), on small spatial scales, basal processes are controlled by the same, fundamental physical mechanisms. We suggest that these mechanisms involve complex feedbacks between ice flow and subglacial environments with a possibility of the ribs being formed in response to ice flow. The similarity in size of the inverted basal shear stress patterns with certain geomorphological features formed by former large ice sheets suggests that these physical mechanisms are not exclusive to the present-day ice sheets and are universal to past, present, and potential future ice sheets experiencing sliding at their bases. The widespread presence of the rib-like structures on the present-day ice sheets is indicative of the substantial basal sliding occurring at their base. The organized patterns of these structures points to their origin via a dynamic instability, and their potential evolution on decadal time scales. Establishing the mechanisms and physical processes controlling the formation and evolution of the basal rib-like patterns is fundamental to understanding the basic nature of ice sheet behavior and robust projections of their future evolution.

Acknowledgments

We thank the Editor and two anonymous referees for thorough reviews, constructive criticisms, and useful suggestions that substantially improved the manuscript. O.V.S. is supported by awards NA08OAR4320752 and NA13OAR439 from the National Oceanic and Atmospheric Administration, U.S. Department of Commerce. The statements, findings, conclusions, and recommendations are those of the author and do not necessarily reflect the views of the National Oceanic and Atmospheric Administration, or the U.S. Department of Commerce. T.T.C. was supported by NSF grant OPP-1043481. R.C.A.H. was funded by the British Antarctic Survey Polar Science for Planet Earth program. The results of this study will be available at NSIDC.

The Editor thanks two anonymous reviewers for their assistance in evaluating this paper.

References

Bamber, J., J. L. Gomez-Dans, and J. A. Griggs (2009), *Antarctic 1 km Digital Elevation Model (DEM) From Combined ERS-1 Radar and ICESat Laser Satellite Altimetry*, National Snow and Ice Data Center, Boulder, Colo.

Bamber, J. L., et al. (2013), A new bed elevation dataset for Greenland, *Cryosphere*, *7*, 499–510, doi:10.5194/tc-7-499-2013.

Catania, G. A., and T. A. Neumann (2010), Persistent englacial drainage features in the Greenland ice sheet, *Geophys. Res. Lett.*, *37*, L02501, doi:10.1029/2009GL041108.

Clark, C. D. (2010), Emergent drumlins and their clones: From till dilatancy to flow instabilities, *J. Glaciol.*, *56*(200), 1011–1025.

Cofaigh, C., J. Dowdeswell, C. Allen, J. Hiemstra, C. Pudsey, J. Evans, and D. Evans (2005), Flow dynamics and till genesis associated with a marine-based antarctic palaeo-ice stream, *Quat. Sci. Rev.*, *24*(5-6), 709–740, doi:10.1016/j.quascirev.2004.10.006.

Creyts, T. T., G. K. C. Clarke, and M. Church (2013), Evolution of subglacial overdeepenings in response to sediment redistribution and glaciohydraulic supercooling, *J. Geophys. Res. Earth Surf.*, *118*, 423–446, doi:10.1002/jgrf.20033.

Dahl-Jensen, D., et al. (2013), Eemian interglacial reconstructed from a Greenland folded ice core, *Nature*, *493*(7433), 489–494, doi:10.1038/nature11789.

Dunlop, P., C. D. Clark, and R. C. A. Hindmarsh (2008), The Bed Ribbing Instability Explanation (BRIE)—Testing a numerical model of ribbed moraine formation arising from coupled flow of ice and subglacial sediment, *J. Geophys. Res.*, *113*, F03005, doi:10.1029/2007JF000954.

Engelhardt, H., and B. Kamb (1997), Basal hydraulic system of a West Antarctic ice stream: Constraints from borehole observations, *J. Glaciol.*, *43*(2), 207–230.

Engelhardt, H., N. Humphrey, B. Kamb, and M. Fahnestock (1990), Physical conditions at the base of a fast moving Antarctic ice stream, *Science*, *248*(4951), 57–59.

Fretwell, P., et al. (2013), Bedmap2: Improved ice bed, surface and thickness datasets for Antarctica, *Cryosphere*, *7*, 375–393, doi:10.5194/tc-7-375-2013.

Goldberg, D. N., and O. V. Sergienko (2011), Data assimilation using a hybrid ice flow model, *Cryosphere*, *5*, 315–327.

Greenwood, S. L., and J. Kleman (2010), Glacial landforms of extreme size in the Keewatin sector of the Laurentide Ice Sheet, *Quat. Sci. Rev.*, *29*, 1894–1910.

Gudmundsson, G. H. (2003), Transmission of basal variability to a glacier surface, *J. Geophys. Res.*, *108*(B5), 2253, doi:10.1029/2002JB002107.

Hindmarsh, R. C. A. (1998), The stability of a viscous till sheet coupled with ice flow, considered at wavelengths less than the ice thickness, *J. Glaciol.*, *44*(147), 285–292.

Iverson, N. R. (2010), Shear resistance and continuity of subglacial till: Hydrology rules, *J. Glaciol.*, *56*(200), 1104–1114.

Joughin, I., S. Tulaczyk, D. MacAyeal, and H. Engelhardt (2004), Melting and freezing beneath the Ross ice streams, Antarctica, *J. Glaciol.*, *50*, 96–108.

Joughin, I., B. Smith, I. Howat, T. Moon, and T. Scambos (2010), Greenland flow variability from ice-sheet-wide velocity mapping, *J. Glaciol.*, *56*(197), 415–430, doi:10.3189/002214310792447734.

King, E. C., J. Woodward, and A. M. Smith (2007), Seismic and radar observations of subglacial bed forms beneath the onset zone of Rutford Ice Stream Antarctica, *J. Glaciol.*, *53*(183), 665–672, doi:10.3189/002214307784409216.

MacAyeal, D. R. (1992), The basal stress-distribution of Ice Stream-E, Antarctica, inferred by control methods, *J. Geophys. Res.*, *97*(B1), 595–603.

Meierbachtol, T., J. Harper, and N. Humphrey (2013), Basal drainage system response to increasing surface melt on the Greenland ice sheet, *Science*, *341*(6147), 777–779, doi:10.1126/science.1235905.

Nitsche, F. O., K. Gohl, R. D. Larter, C. D. Hillenbrand, G. Kuhn, J. A. Smith, S. Jacobs, J. B. Anderson, and M. Jakobsson (2013), Paleo ice flow and subglacial meltwater dynamics in Pine Island Bay, West Antarctica, *Cryosphere*, *7*(1), 249–262, doi:10.5194/tc-7-249-2013.

Oswald, G. K. A., and S. P. Gogineni (2012), Mapping basal melt under the Northern Greenland ice sheet, *IEEE Trans. Geosci. Remote Sens.*, *50*(2), 585–592, doi:10.1109/TGRS.2011.2162072.

Peters, L. E., S. Anandakrishnan, R. B. Alley, J. P. Winberry, and D. E. Voigt (2006), Subglacial sediments as a control on the onset and location of two Siple Coast ice streams, West Antarctica, *J. Geophys. Res.*, *111*, B01302, doi:10.1029/2005JB003766.

Rignot, E., J. Mouginot, and B. Scheuchl (2011), Ice flow of the Antarctic ice sheet, *Science*, *333*(6048), 1427–1430, doi:10.1126/science.1208336.

Schoof, C. (2002), Basal perturbations under ice streams: Form drag and surface expression, *J. Glaciol.*, *48*(162), 407–416.

Schroeder, D. M., D. D. Blankenship, and D. A. Young (2013), Evidence for a water system transition beneath Thwaites Glacier, West Antarctica, *PNAS*, *110*(30), 12,225–12,228, doi:10.1073/pnas.1302828110.

Sergienko, O. V. (2012), The effects of transverse bed topography variations in ice-flow models, *J. Geophys. Res.*, *117*, F03011, doi:10.1029/2011JF002203.

Sergienko, O. V. (2013), Glaciological twins: Basally controlled subglacial and supraglacial lakes, *J. Glaciol.*, *59*(213), 3–8, doi:10.3189/2013JoG12J040.

Sergienko, O. V., and R. C. A. Hindmarsh (2013), Regular patterns in frictional resistance of ice-stream beds seen by surface data inversion, *Science*, *342*(6162), 1086–1089, doi:10.1126/science.1243903.

Sergienko, O. V., R. A. Bindschadler, P. L. Vornberger, and D. R. MacAyeal (2008), Ice stream basal conditions from block-wise surface data inversion and simple regression models of ice stream flow: Application to Bindschadler Ice Stream, *J. Geophys. Res.*, *113*, F04010, doi:10.1029/2008JF001004.

Shreve, R. (1972), Movement of water in glaciers, *J. Glaciol.*, *11*(62), 205–214.

Smalley, I. J., and D. J. Unwin (1968), The formation and shape of drumlins and their distribution and orientation in drumlin fields, *J. Glaciol.*, *7*(51), 377–390.

Smith, A., T. Murray, K. Nicholls, K. Makinson, G. Algeirsdóttir, A. Behar, and D. Vaughan (2007), Rapid erosion, drumlin formation, and changing hydrology beneath an Antarctic Ice Stream, *Geology*, *35*, 127–130.

Tulaczyk, S., R. P. Scherer, and C. D. Clark (2001), A ploughing model for the origin of weak tills beneath ice streams: A qualitative treatment, *Quat. Int.*, *86*, 59–70.

Van der Veen, C. J. (1999), *Fundamentals of Glacier Dynamics*, 472 pp. 1st ed., Taylor & Francis, Rotterdam, Netherlands.

Wingham, D. J., M. J. Siegert, A. Shepherd, and A. S. Muir (2006), Rapid discharge connects Antarctic subglacial lakes, *Nature*, *440*, 1033–1036, doi:10.1038/nature04660.

Wolovick, M. J., R. E. Bell, T. T. Creyts, and N. Frearson (2013), Identification and control of subglacial water networks under Dome A, Antarctica, *J. Geophys. Res. Earth Surf.*, *118*, 140–154, doi:10.1029/2012JF002555.